Electronic Supplementary Material (ESI) for Inorganic Chemistry Frontiers.

Supporting information

Understanding the synergistic effect of piezoelectric polarization and extra electrons contributed by oxygen vacancies on efficient piezo-photocatalysis CO_2 reduction

Qijun Xu, Jingwen Jiang, Xuelin Sheng, Qi Jing, Xiaofeng Wang, Lingyan Duan*(iD 0000-0003-3446-0112), Hong Guo*(iD 0000-0001-5693-2980)

International Joint Research Center for Advanced Energy Materials of Yunnan Province, Yunnan Key Laboratory of Carbon Neutrality and Green Low-carbon Technologies, School of Materials and Energy, Yunnan University, Kunming 650091, China

e-mail: lingyan.duan@ynu.edu.cn, guohong@ynu.edu.cn

S1 Experimental section

Materials.

Bismuth nitrate pentahydrate ($Bi(NO_3)_3·5H_2O$, 99.99%), Ferric nitrate nonahydrate ($Fe(NO_3)_3·9H_2O$, 99.9%), Nitric acid (HNO_3, AR), Potassium hydroxide (KOH, 99.99%), Ethanol (C_2H_6O, AR 99.7%), Sodium borohydride ($NaBH_4$, 99%), Others solvents, reagents and chemicals were used without further purification.

Synthesis of $BiFeO_3$. First, dissolve 1.6797 g of $Bi(NO_3)_3·5H_2O$ and 1.4141 g of $Fe(NO_3)_3·9H_2O$ in 20ml, 1 mol/L dilute nitric acid solution. Use a magnetic stirrer to continuously stir the solution. After the solution is completely dissolved, add 52.5 ml, 4 mol/L KOH solution to the solution drop by drop, and the solution gradually turns into a dark brown suspension. In order to mix the solution evenly, put the solution into the ultrasonic cleaning instrument for ultrasonic treatment for 8 min, and continue to stir the solution with a magnetic stirrer for 30 min. Then pour the prepared precursor into 100 ml Teflon lining, put the Teflon lining into the reaction kettle and put it into the constant temperature drying oven. After reacting at 200 ℃ for 6 h, the reactor was naturally cooled to room temperature. After dismantling the reactor, remove the supernatant in the PTFE lining, wash the product with distilled water and absolute ethanol for several times, and dry it in a vacuum drying oven at 80 ℃ for 12 h, and finally get $BiFeO_3$ product.

Synthesis of $BiFeO_{3-x}$. Weigh 0.5 g $BiFeO_3$ and 0.2 g $NaBH_4$ respectively, mix the two powders in a mortar and grind them for 10~30 min. After it is fully mixed, put the sample into the porcelain boat and put it in the tubular furnace, and then install the tubular furnace. Turn on the vacuum pump and vacuum the tubular furnace until the pressure gauge shows -0.1 mpa. Turn off the vacuum pump. At this time, the inside of the furnace tube is in a vacuum state. Open the argon valve, then open the air inlet of the tubular furnace, and then open the air outlet when the pressure gauge shows 0. At this time, bubbles can be seen in the conical bottle, about one bubble per second, indicating that the gas path is unobstructed. Then, close the door of the tubular furnace and set the heating parameters. The heating rate is 5 ℃/min, heated to 300 ℃, and kept warm for 120 min. After the program is set, start the program so that the tubular furnace begins to heat up. After the tubular furnace procedure is completed and cooled naturally to room temperature, disassemble the tubular furnace and pour the sintered powder sample onto the weighing paper. Use a beaker to measure 50 ml of absolute ethanol, and then pour the above samples into absolute ethanol to disperse for 2 h. Then, the dispersed samples are divided into two centrifuge tubes, with a calibration mass difference of 0.1 g, centrifuged at a speed of 8000 r/min for 3 min each time, washed twice with alcohol, and then washed several times with deionized water until the pH value is neutral. The purpose of this process is to wash away the excess $NaBH_4$ mixed in $BiFeO_{3-x}$. Put the cleaned samples into a vacuum drying oven and dry them under vacuum for 12 h at a temperature of 60 ℃. The dried sample is then ground to obtain $BiFeO_{3-x}$ sample.

S2 Characterization

TEM images and the high-resolution images are recorded using a high-resolution transmission electron microscope (HRTEM, JEM-2010). The morphology of samples is investigated using scanning electron microscope (SEM) (AMRAY 1000B), the elements distribution is detected by SEM EDS mapping. The Powder X-ray diffraction (PXRD) patterns of the samples are obtained using a X-ray diffractometer with Copper target Kα radiation (λ = 1.5418 nm), scanning range (Angle 2θ) of 10°~ 90°, scanning time of 0.5 s. The unpaired electrons in the atoms or molecules of the sample to see whether vacancy phenomena are produced by Electron Paramagnetic Resonance (EPR) (A300, Bruker Daltonics, U.S.A.). Elements content is evaluated by X-ray photoelectron spectroscopy (XPS) recorded by K-Alpha+ (Thermo Fisher Scientific, U.S.A.) where the source of radiation was mono Al Kα. The photo luminescence (PL) and time-resolved PL decay measurements are conducted on a fluorescence spectrometer (PF5301PC, Shimadzu, Japan) using a Xenon lamp (excitation at 330 nm) as a light source. UV–visable diffuse reflectance spectra (DRS) are obtained using a Shimadzu UV-2700 recording spectrophotometer.

S3 EPR measurements

EPR identification of oxygen vacancies was operated at room temperature. TEMP (2,2,6,6-tetramethyl-1-piperidine) and DMPO (5, 5-dimethyl-l-pyrroline N-oxide) was used as spin-trapping reagent.

S4 In-situ DRIFTS analyses for CO_2 photoreduction

In-situ DRIFTS (diffuse reflectance infrared Fourier transform spectra) tests were conducted on Nicolet iS50FT-IR spectrometer (Thermo Fisher, USA) equipped with a designed reaction chamber and a liquid water cooling HgCdTe (MCT) detector. The sample along with a Cu holder was put into the reaction chamber. Then the sample was purged with N_2 (30 mL/min) for 1 h at 100°C to blow out all the gases in the cell and adsorbed on the samples. After the reaction chamber cooling down to room temperature, the mixture of CO_2 (5 mL/min) and H_2O vapor were introduced into the chamber for 30 min to make sure the sorption equilibrium before irradiation.

S5 SPV measurements

SPV spectra were obtained based on a lock-in amplifier. The measurement systems included a lock-in amplifier, monochromatic light, a light chopper, and a sample chamber. Monochromatic light was induced from a 500w Xe lamp via a monochromator.

S6 EIS measurements

For electrochemical measurements, the working electrodes were prepared as follows: 10 mg of the as-prepared photocatalyst powder was mixed with 10μL Nafion(5%) and 150μL ethanol under sonication for 1 h to produce a slurry, which was then drop-cast onto a half of indium-tin oxide (ITO) conductive glass with a fixed active area of 1.0×2.0 cm^2. The prepared electrodes were allowed to dry at room temperature for 10 h. The photoelectrochemical properties and EIS tests of the catalyst were carried out on the Princeton Applied Research P3000A. The electrochemical performance test was carried out in an electrolytic cell of a three-electrode system. The ITO coated with photocatalyst sample was the working electrode, the Ag/AgCl (saturated KCl) electrode was used as the reference electrode, the Pt sheet is the counter electrode, and 0.1 M sodium sulfate solution was used as the electrolyte solution. All test experiments are carried out at room temperature. During the EIS test, the applied bias voltage is 0 V, and the open circuit potential frequency range is 10^5 Hz to 10^{-1} Hz.

S7 Calculation method of energy band structure

As shown in Fig. 4e, the negative slope of Mott-Schottky curve shows that $BiFeO_3$ and $BiFeO_{3-x}$ are P-type semiconductors. The flat band potentials (E_{fb}) of $BiFeO_3$ and $BiFeO_{3-x}$ are 0.38 and 0.43 V vs. Ag/AgCl (-0.1, -0.058 and -0.08 V vs. NHE), respectively [1,2]. Subsequently, the CB of $BiFeO_3$ and $BiFeO_{3-x}$ are estimated to be 0.38 and 0.43 V vs. NHE, respectively. The VB of $BiFeO_3$ and $BiFeO_{3-x}$ can be estimated by E_g and EVB, which are 2.58 and 2.58 eV, respectively. The distance from the VB to the E_f can be determined by the VB-XPS of $BiFeO_3$ and $BiFeO_{3-x}$ (Fig. 4g) [3-5].

S8 In-situ DRIFTS analyses for CO_2 photoreduction

In-situ DRIFTS (diffuse reflectance infrared Fourier transform spectra) tests were conducted on Nicolet iS50 FT-IR spectrometer (Thermo Fisher, USA) equipped with a designed reaction chamber and a liquid water cooling HgCdTe (MCT) detector. The sample along with a Cu holder was put into the reaction chamber. Then the sample was purged with N_2 (30 mL/min) for 1 h at 100°C to blow out all the gases in the cell and adsorbed on the samples. After the reaction chamber cooling down to room temperature, the mixture of CO_2 (5 mL/min) and H_2O vapor were introduced into the chamber for 30 min to make sure the sorption equilibrium before irradiation.

S9 Measurement of piezo-photocatalysis activity

The CO_2 reduction on the catalyzer in the presence of H_2O was conducted in the LabSolar-IIIAG on-line catalysis analysis system (Beijing Perfectlight). The piezo-photocatalysis CO_2 reduction was carried out in a 50 mL Pyrex reactor. Ultrahigh-purity CO_2 (99.99%) was fed continuously into the reactor at a rate of 0.1 L min^{-1} for 2 h to remove oxygen in the water and saturate the solution. 12 mg of sample was uniformly dispersed in the mixture of 2 mL of deionized water, 22 mL acetonitrile and 6 mL triethanolamine by ultrasonication, and the temperature was kept at 25°C constant by a running water system. The piezo-photocatalysis activity was studied using a 300 W Xe lamp with 420 nm cut-off filter as the visible light source and a 100 Hz ultrasonic instrument. The gas product (1 μL, taken from the reactor) was analyzed using a gas chromatograph (GC-950) equipped with a FID and a TCD detector. Only the products of CO and CH_4 were detected.

Tab. S1 The calculated Eg, EVB and ECB of $BiFeO_3$ and $BiFeO_{3-x}$ samples.

	E_{CB}/eV	Eg/eV	E_{VB}/eV
$BiFeO_3$	0.38	2.2	2.58
$BiFeO_{3-x}$	0.43	2.15	2.58

Tab. S2 Comparison of catalytic activity between $BiFeO_{3-x}$ and reported catalysts for CO_2 reduction.

catalyzer	Type of catalysis	CH_4	CO	Ref
$BiFeO_3$	Piezo-photocatalysis	9.1 (μmol/g)	53.6 (μmol/g)	This work
$BiFeO_{3-x}$	Piezo-photocatalysis	32.8 (μmol/g)	142.6 (μmol/g)	This work
$BaTiO_3$	Piezoelectric catalysis	/	63.3 (μmol/g)	[6]
P25-TiO_2	Photocatalysis	/	7.1 (μmol/g/h)	[7]
Ti_2O_3 / TiO_2	Photocatalysis	0.65 (μmol/g/h)	2.64 (μmol/g/h)	[8]
CdS-P25/ZIF-67	Photocatalysis	1.58 (μmol/h)	1.49 (μmol/h)	[9]
P-CeO_2/g-C_3N_4	Photocatalysis	/	0.523 (μmol/g/h)	[10]
Ti_3C_2/Bi_2WO_6 2D/2D	Photocatalysis	1.78 (μmol/g/h)	/	[11]
TiO_2/GDY	Photocatalysis	2.1 (μmol/g/h)	14.5 (μmol/g/h)	[12]
Fe/PSs	Photocatalysis	/	16 (μmol/g)	[13]

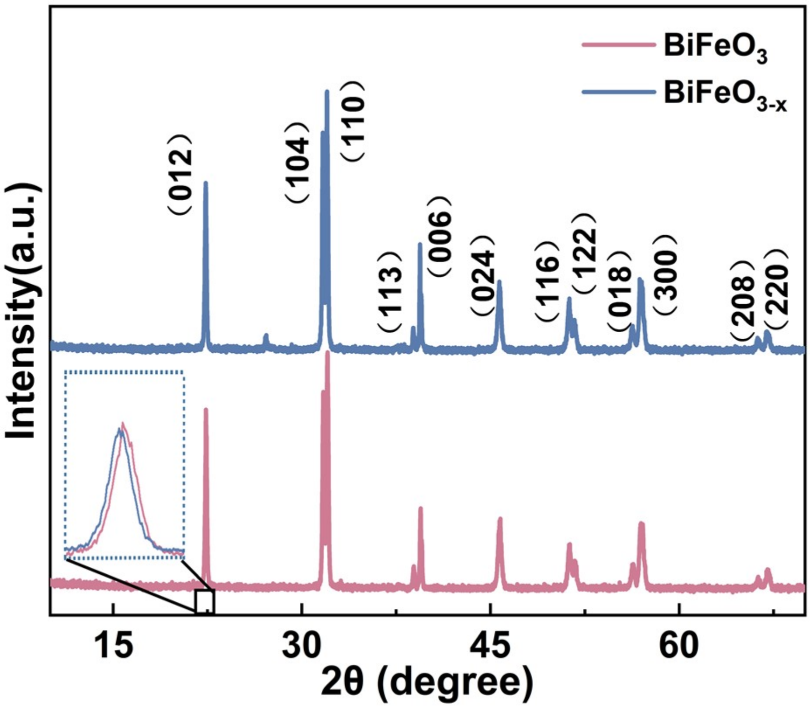

Fig. S1. XRD patterns of $BiFeO_3$ and $BiFeO_{3-x}$.

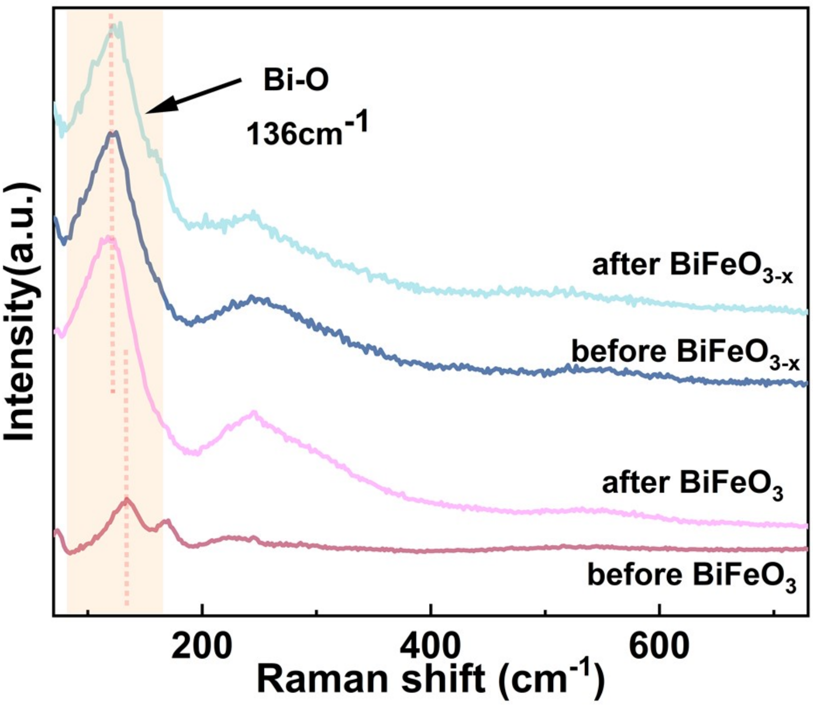

Fig. S2. Raman spectra of before and after piezo-photocatalysis for $BiFeO_3$ and $BiFeO_{3-x}$.

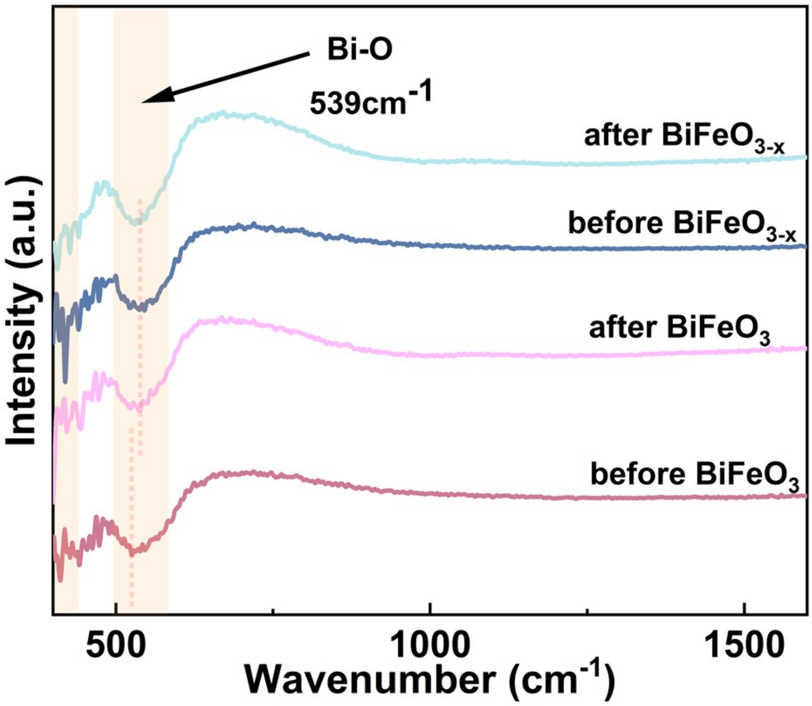

Fig. S3. FT-IR pattern of before and after piezo-photocatalysis for $BiFeO_3$ and $BiFeO_{3-x}$.

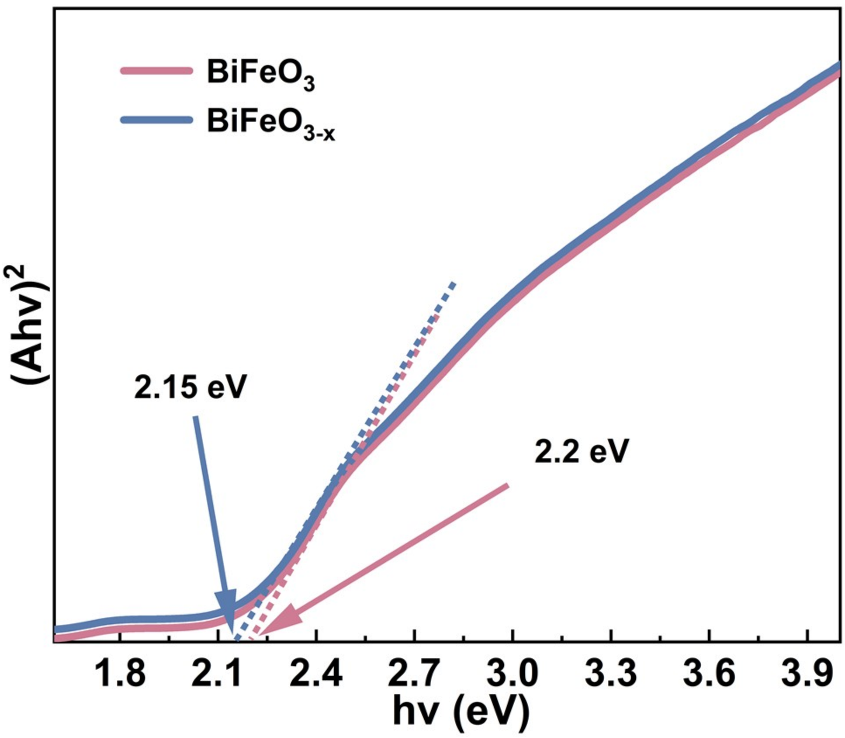

Fig. S4. The band gap width of $BiFeO_3$ and $BiFeO_{3-x}$ catalysts.

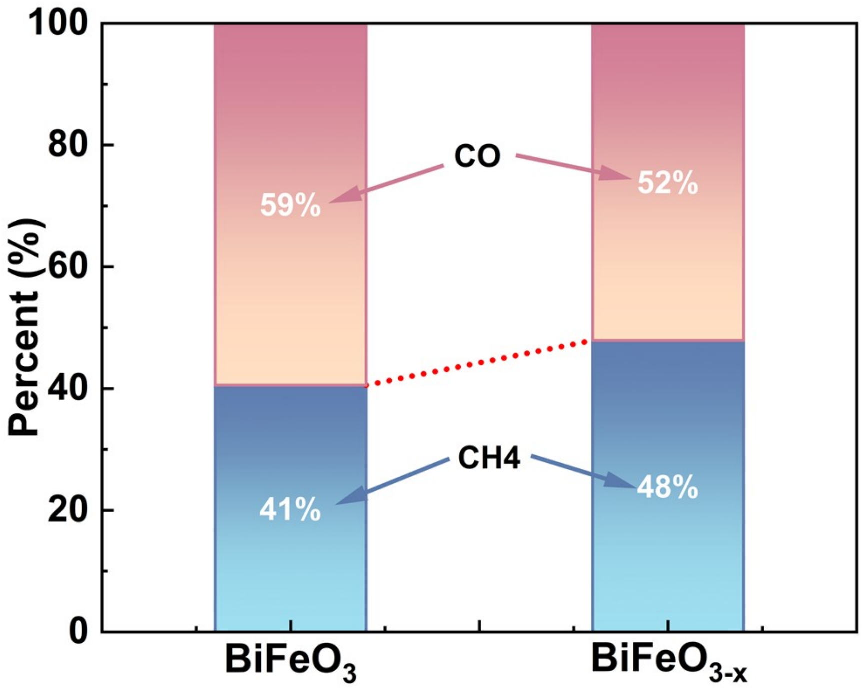

Fig. S5. The selectivity of $BiFeO_3$ and $BiFeO_{3-x}$ catalysts for CO and CH4 at 9 h of piezo-photocatalysis.

Product selectivity is one of the important parameters for reflecting piezo-photocatalysts performance for CO_2 reduction. After discussion, we calculated the selectivity of the product CO and CH_4 according to the following equation [14-17].

$$Selectivity\ for\ CO = \frac{2R(CO)}{8R(CH_4) + 2R(CO)} \times 100\%$$

$$Selectivity\ for\ CH_4 = \frac{8R(CH_4)}{8R(CH_4) + 2R(CO)} \times 100\%$$

Where R(CO) and $R(CH_4)$ are the yields of reactively-formed CO and CH_4 respectively. As can be seen from the calculation results in **Fig. S5**, the introduction of oxygen vacancies improves the product selectivity of $BiFeO_3$ for the piezo-photocatalysis reduction of CO_2 to CH_4. The selectivity of $BiFeO_{3-x}$ for CH_4 is up to 48%.

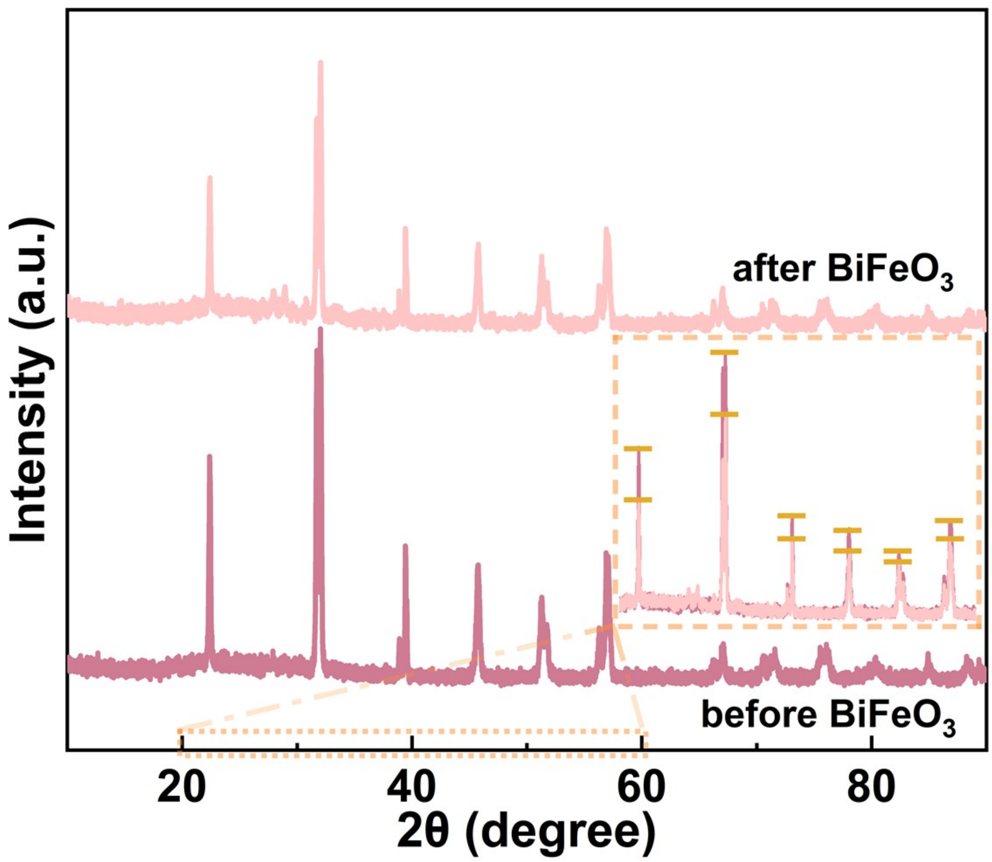

Fig. S6. The XRD patterns of before and after piezo-photocatalysis for $BiFeO_3$.

References

1 K. Chen, T.-T. Jiang, T.-H. Liu, J. Yu, S. Zhou, A. Ali, S.-H. Wang, Y. Liu, L.-X. Zhu, X.-L. Xu, Zn Dopants Synergistic Oxygen Vacancy Boosts Ultrathin CoO Layer for CO_2 Photoreduction, Adv. Funct. Mater., 2022, **32**, 2109336.

2 Z.-R. Miao, Q.-L. Wang, Y.-F. Zhang, L.-P. Meng, X.-X. Wang, In situ construction of S-scheme AgBr/BiOBr heterojunction with surface oxygen vacancy for boosting photocatalytic CO_2 reduction with H_2O, Appl. Catal. B: Envir., 2022, **301**, 120802.

3 A. Hezam, K. Namratha, Q.-A. Drmosh, D. Ponnamma, J.-W. Wang, S. Prasad, M. Ahamed, C. Cheng, and K. Byrappa, CeO_2 Nanostructures Enriched with Oxygen Vacancies for Photocatalytic CO_2 Reduction, ACS Appl. Nano Mater., 2019, **3**, 138-148.

4 Y. Huo, J.-F. Zhang, K. Dai, C.-H. Liang, Amine-Modified S-Scheme Porous g-C_3N_4/CdSe–Diethylenetriamine Composite with Enhanced Photocatalytic CO_2 Reduction Activity, ACS Appl. Energy Mater., 2021, **4**, 956-968.

5 F.-Q. Zhang, L. Zhao, H. Chen, Y.-H. He, P. Tian, X.-H. Zeng, Synthesis of mesoporous Fe/h-CeO_2 hollow micro-spheres with enhanced visible light photocatalytic activity, Mater. Res. Express., 2019, **6**, 095516.

6 J.-P. Ma, S.-J. Jing, Y. Wang, X. Liu, L.-Y. Gan, C. Wang, J.-Y. Dai, X.-D. Han, X.-Y. Zhou, Piezo-electrocatalysis for CO_2 reduction driven by vibration, Adv. Energy Mater., 2022, **12**, 2200253.

7 Z. Mo, X.-W. Zhu, Z.-F. Jiang, Y.-H. Song, D.-B. Liu, H.-P. Li, X.-F. Yang, Y.-B. She, Y.-C. Lei, S.-Q. Yuan, H.-M. Li, L. Song, Q.-Y. Yan, H. Xu, Porous nitrogen-rich g-C_3N_4 nanotubes for efficient photocatalytic CO_2 reduction, Appl. Catal. B Environ., 2019, **256**, 117854.

8 M. Xu, A. Zada, R. Yan, H.-N. Li, N. Sun, Y. Qu, Ti_2O_3/TiO_2 heterophase junctions with enhanced charge separation and spatially separated active sites for photocatalytic CO_2 reduction. Phys Chem Chem Phys., 2020, **22**, 4526-4532.

9 L. Wang, Z.-T. Zhang, Q. Han, Y. Liu, J.-B. Zhong, J.-F. Chen, J.-W. Huang, H.-D. She, Q.-Z. Wang, Preparation of CdS-P25/ZIF-67 composite material and its photocatalytic CO_2 reduction performance. Appl. Surf. Sci., 2022, **584**, 152645.

10 W. Li, L. Jin, F. Gao, H. Wan, Y. Pu, X. Wei, C. Chen, W. Zou, C. Zhu, L. Dong, Advantageous roles of phosphate decorated octahedral $CeO_2\{111\}$/g-C_3N_4 in boosting photocatalytic CO_2 reduction: charge transfer bridge and lewis basic site,

Appl. Catal. B Environ., 2021, **294**, 120257.

11 S.-W. Cao, B.-J. Shen, T. Tong, J.-W. Fu, J.-G. Yu, 2D/2D heterojunction of ultrathin MXene/Bi_2WO_6 nanosheets for improved photocatalytic CO_2 reduction, Adv. Funct. Mater., 2018, **28**, 1800136.

12 F.-Y. Xu, K. Meng, B.-C. Zhu, H.-B. Liu, J.-S. Xu, and J.-G. Yu, Graphdiyne: A New Photocatalytic CO_2 Reduction Cocatalyst, Adv. Funct. Mater., 2019, **29**, 1904256.

13 Q.-Q. Lei, H.-Q. Yuan, J.-H. Du, M. Ming, S. Yang, Y. Chen, J.-X. Lei, Z.-J. Han, Photocatalytic CO_2 reduction with aminoanthraquinone organic dyes, Nat. Commun., 2023, **14**, 1087.

14 Y. Zhang, W. Chen, M. Zhou, G. Miao, Y. Liu, Efficient Photocatalytic CO_2 Reduction by the Construction of Ti_3C_2/ $CsPbBr_3$ QD Composites, ACS Appl. Energy Mater., 2021, **4,** 9154-9165.

15 S. Kumar, M. Isaacs, R. Trofimovaite, L. Durndell, C. Parlett, R. Douthwaite, B. Coulson, M. Cockett, K. Wilson, A. Lee, P25@CoAl layered double hydroxide heterojunction nanocomposites for CO_2 photocatalytic reduction, Appl. Catal. B Environ., 2017, **209**, 394-404.

16 R. Bhosale, S. Jain, C. Vinod, S. Kumar, S. Ogale, Direct Z-Scheme g-C_3N_4/$FeWO_4$ Nanocomposite for Enhanced and Selective Photocatalytic CO_2 Reduction under Visible Light, ACS Appl. Mater. Interfaces., 2019, **11**, 6174-6183.

17 S. Tonda, S. Kumar, M. Bhardwaj, P. Yadav, S. Ogale, g-C_3N_4/NiAl-LDH 2D/2D Hybrid Heterojunction for High-Performance Photocatalytic Reduction of CO_2 into Renewable Fuels, ACS Appl. Mater. Interfaces., 2018, **10**, 2667-2678.